University of Reading

The equivalent barotropic structure of waves in the tropical atmosphere in the Western Hemisphere

Article

Published Version

Creative Commons: Attribution 4.0 (CC-BY)

Open access

Yang, G. -Y. ORCID: https://orcid.org/0000-0001-7450-3477 and Hoskins, B. (2017) The equivalent barotropic structure of waves in the tropical atmosphere in the Western Hemisphere. Journal of the Atmospheric Sciences, 74 (6). pp. 1689-1704. ISSN 1520-0469 doi: 10.1175/JAS-D-16-0267.1 Available at https://centaur.reading.ac.uk/69285/

It is advisable to refer to the publisher's version if you intend to cite from the work. See Guidance on citing.

To link to this article DOI: http://dx.doi.org/10.1175/JAS-D-16-0267.1

Publisher: American Meteorological Society

All outputs in CentAUR are protected by Intellectual Property Rights law, including copyright law. Copyright and IPR is retained by the creators or other copyright holders. Terms and conditions for use of this material are defined in the End User Agreement.

www.reading.ac.uk/centaur

University of Reading

CentAUR

Central Archive at the University of Reading

Reading's research outputs online

The Equivalent Barotropic Structure of Waves in the Tropical Atmosphere in the Western Hemisphere

GUI-YING YANG

National Centre for Atmospheric Science, and University of Reading, Reading, United Kingdom

BRIAN J. HOSKINS

University of Reading, Reading, and Grantham Institute for Climate Change, Imperial College, London, United Kingdom

(Manuscript received 15 September 2016, in final form 5 January 2017)

ABSTRACT

Tropical waves are generally considered to have a baroclinic structure. However, analysis of ERA-Interim and NOAA OLR data for the period 1979–2010 shows that in the equatorial and Northern Hemisphere near-equatorial regions in the tropical Western Hemisphere (WH), westward- and eastward-moving transients, with zonal wavenumbers 2–10 and periods of 2–30 days, have little tilt in the vertical and can be said to be equivalent barotropic. The westward-moving transients in the equatorial region have large projections onto the westward mixed Rossby–gravity (WMRG) wave and those in the near-equatorial region project onto the gravest Rossby wave and also the WMRG. The eastward-moving transients have large projections onto the Doppler-shifted eastward-moving versions of these waves.

To examine how such equivalent barotropic structures are possible in the tropics, terms in the vorticity equation are analyzed. It is deduced that waves must have westward intrinsic phase speeds and can exist in the WH with its large westerly vertical shear. Throughout the depth, the advection of vorticity by the zonal flow and the β term are large and nearly cancel. In the upper troposphere the zonal advection by the strong westerly flow wins and the residual is partially balanced by vortex shrinking associated with divergence above a region of ascent. Below the region of ascent the β term wins and is partially balanced by vortex stretching associated with the convergence. An equivalent barotropic structure is therefore maintained in a similar manner to higher latitudes. The regions of ascent are usually associated with deep convection and, consistently, WH waves directly connected to tropical convection are also found to be equivalent barotropic.

1. Introduction

Large-scale structures in extratropical regions have long been known to have an equivalent barotropic structure in the vertical, with little tilt in wind and pressure field anomalies with height. Midlatitude weather systems also generally have relatively small vertical tilts, except when growing rapidly. However, since Gill (1980), the general picture of equatorial waves, along with most other tropical disturbances, is that they are dominated by a baroclinic structure with horizontal velocity and pressure fields having opposite signs in the upper and lower troposphere. This is based on the first internal mode in a theoretical model including a rigid tropopause lid. It is also based on a simple conceptual model with deep convective latent heating largely balanced by adiabatic cooling associated with ascent, implying upper-tropospheric vortex shrinking and lower-tropospheric vortex stretching. Advection by any ambient zonal flow is assumed to be unimportant. As will be shown in this paper, the missing ingredient in this perspective is the strongly sheared tropical zonal wind.

Some modeling studies have shown that the vertical shear of the zonal flow allows tropical waves to have both baroclinic and barotropic components. However,

Denotes content that is immediately available upon publication as open access.

Corresponding author e-mail: Gui-Ying Yang, g.y.yang@reading.ac.uk

DOI: 10.1175/JAS-D-16-0267.1

This article is licensed under a Creative Commons Attribution 4.0 license (http://creativecommons.org/licenses/by/4.0/).

© 2017 American Meteorological Society

the barotropic component generally emanates poleward into the extratropics and has a smaller amplitude in the tropics compared with the baroclinic component (e.g., Kasahara and Silva Dias 1986; Wang and Xie 1996). Therefore the simulated tropical waves are dominated by a baroclinic structure.

There have been exceptions to this view. The scale analysis of Charney (1963) suggested that away from regions of condensational heating the flow will be quasi horizontal and quasi nondivergent, and therefore the motion at any level will be described by the barotropic vorticity equation. Given the evidence in Yanai et al. (1968) and Wallace and Kousky (1968) that observed waves in the troposphere and stratosphere had a strongly coupled vertical structure, Holton (1969) challenged the relevance of the result of Charney's analysis, which depended on the assumption of a vertical scale for the motion on the order of the scale height, ~10 km. However Nishi (1989) found that 30–60-day variability in the India–Central America sector exhibited little phase tilt in the vertical. Also the scale analysis of Yano and Bonazzola (2009) showed that various regimes were possible.

Observed equatorial Kelvin waves do indeed show a "classic" baroclinic structure. The westward-moving mixed Rossby–gravity (WMRG) and meridional mode number $n = 1$ Rossby (R1) waves in the Eastern Hemisphere are also dominated by a baroclinic structure (e.g., Wheeler et al. 2000; Yang et al. 2007a; Kiladis et al. 2009; Yang et al. 2011, 2012). However, a number of observational studies indicate that in the Western Hemisphere (WH) WMRG waves have a rather deep vertical structure (Yang et al. 2011, 2012) and R1 waves are predominantly barotropic, especially in boreal winter (e.g., Kiladis and Wheeler 1995; Yang et al. 2007a; Kiladis et al. 2009; Yang et al. 2011, 2012).

It will be shown in this paper that the transient motions in the east Pacific and Atlantic in boreal winter in both an equatorial (10°S–10°N) and Northern Hemisphere (NH) near-equatorial (10°–20°N) bands have a vertical structure that is essentially equivalent barotropic. This is the case for the westward-moving features and also for eastward-moving features. The main aim of this paper is to present the structures that are present in the latitude bands and show how such barotropic structures are dynamically consistent. A subsidiary aim is to show their relationship to the WMRG and R1 waves.

The outline of this paper is as follows. Section 2 describes the data and methodology used in this study. Section 3 presents the climatological-mean vertical structures of the waves in the two latitude bands in the WH. It also shows the relationship to WMRG and R1 waves and to the Doppler-shifted eastward-moving WMRG-E[1] and R1-E waves and displays the vertical structures of these. A general analysis of the conditions for waves to have an equivalent barotropic structure to be possible in the tropics is given in section 4. In section 5 the relevance of this analysis to the observed waves, and the terms in the vorticity equation for them are discussed. Section 6 gives a summary and also a brief discussion of the barotropic behavior of the waves in the two latitude bands that are directly related to convection.

2. Data and methodology

Data used in this study are ERA-Interim horizontal winds u and v and geopotential height Z for the period from 1979 to 2010. The fields are available 6 hourly with horizontal resolution of about 0.7° and at 37 pressure levels from 1000 to 1 hPa. Detailed information on the data can be found in Dee et al. (2011). As a proxy for convection, NOAA interpolated daily outgoing longwave radiation (OLR), which has a horizontal resolution of 2.5° × 2.5° (Liebmann and Smith 1996), is also used in the final section.

The basic part of the analysis is to separate the primary fields into eastward- and westward-moving components using a space–time spectral analysis and then filter them in a large wavenumber–frequency domain that contains most equatorial wave power: zonal wavenumbers k from 2 to 10 and from −2 to −10 and periods from 2 to 30 days. The filtered variables will be denoted by an asterisk (e.g., v^*), noting that there will be both eastward and westward components of these variables.

Linear regression techniques similar to those used in Yang et al. (2007a,c, 2011, 2012) are used in sections 3, 5, and 6 to obtain wave structures and the associated variables that give the vorticity budget terms. In this study, the independent variable is the extrema in 300-hPa v^* (or OLR* in section 6) in a given longitude range (e.g., 160°–100°W for the east Pacific), averaged in the latitude band of interest (e.g., 10°N–10°S for equatorial band). The required 3D horizontal wind fields for the westward- and eastward-moving transients are obtained by regressing them for each year, at each level and at each latitude onto the independent variable with a longitude shift in terms of their longitudinal relationship to the independent variable, which is taken to be located at 0° relative longitude. After regression, the 3D regressed horizontal wind fields for each year are obtained by taking the independent variable to be positive for the 300-hPa v^* extrema (or negative for OLR* extrema)

[1] Note that this wave is not the intrinsic eastward-moving $n = 0$ EMRG wave.

with a magnitude 1.5 times its peak standard deviation in the region. Finally, the regressed field is averaged for the 31 boreal winters. Investigation shows that the results are almost identical if only positive or only negative extrema in v^* are used as the independent variable for the regression and, also, if the regression is performed on all the extrema for the 31 yr rather than averaging the results for the individual years.

Although equatorial wave modes are not the main focus in this paper, for relating the westward-/eastward-moving transient motions to equatorial wave modes, the westward and eastward fields are separately projected onto the equatorial wave mode structures. The projection method used was developed in Yang et al. (2003) and has been applied in a number of subsequent studies (e.g., Yang et al. 2007a,b,c, 2011, 2012). The projection is done separately at each level, and there is no assumption about the vertical structure or imposition of the dispersion relation. The details for the technique are not given here as the equatorial wave mode aspect is not central to this paper and also the projection technique is fully discussed in the papers mentioned above.

As the equivalent barotropic nature of the wave structure is more significant in the extended boreal winter season (November–April) and all the four waves have strong amplitude over the WH westerly duct regions in the east Pacific (E. Pacific herein) and Atlantic (Hoskins and Yang 2016; Yang and Hoskins 2016), the analysis in this study is focused on this season and hemisphere. Similar behavior is found in the two duct regions, and most of the presentation and discussion of the dynamics involved will be for the E. Pacific.

3. Climatological winter-mean vertical structure of tropical waves

The westward- and eastward-moving transients in an equatorial band, 10°S–10°N, and in a near-equatorial band in the Northern Hemisphere (NH), 10°–20°N, will be investigated. The NH band is chosen because there are strong transients there associated with the ITCZs that are in the NH, and the convective activity maximizes there. Also, as will be shown below, the wave structures are different from those in the equatorial band. The longitude–height structures of the transients in the two bands are obtained by regressing the meridional wind v^* at each level onto the 300-hPa v^* extrema in each band in both the E. Pacific (160°–100°W) and Atlantic (50°–10°W).

Considering first the E. Pacific (Fig. 1a), a wavelike structure is seen for the westward-moving component in the NH band, with extrema near 250 hPa and decreasing to small values near the tropopause and near the surface. Vertical tilts are very small and the structure can clearly be described as equivalent barotropic. The eastward component in the NH band has a similar wavelike and equivalent barotropic structure, but with a slightly shorter wavelength and more confined in the vertical. In the equatorial band the westward component is again wavelike and quite barotropic, though with some westward tilt with height in its upper region and eastward tilt in its lower region. In the equatorial band the eastward-moving structure is similar, but, as with the NH band, it is more confined in the vertical.

Very similar structures in the four categories are found in the Atlantic (Fig. 1b). Also those in the 10°–20°S band (not shown) are similar to, but weaker than, those for 10°–20°N. In the rest of the paper the analysis will focus on the E. Pacific and on the equatorial and NH bands, but the deductions will apply also to the Atlantic and, therefore, to the two regions in the WH with large variance in tropical v.

Figure 1c gives the regressed structure of horizontal divergence D^*, calculated from regressed horizontal winds u^* and v^*, for the E. Pacific. The westward and eastward components for NH band give a clear picture of a node and a reversal in sign near 350 hPa. Near the zero longitude there is divergence in the upper portions of the structures, zero divergence below this, and convergence in the lower portions of the structure, implying a single maximum in ascent. For the waves in the equatorial band a similar structure is apparent, with a reversal in sign near 300 hPa, though the picture is slightly less clear for the westward-moving wave, consistent with its vertical tilts.

To summarize the amplitudes v^* and D^* as a function of height, Fig. 2 gives the root-mean-square (RMS) of both, averaged over the longitude range from −60° to +60°. In each case, whereas v^* shows a simple maximum, there are two maxima for D^* and three minima sandwiching them.

Table 1 summarizes the vertical structures for the four categories, based on the RMS values in the longitude range −60° to +60°. For v^* it gives the levels of maximum amplitudes and the upper and lower levels at which the amplitudes are about 0.1 of the maxima. For D^*, it shows the levels of the upper and lower maximum amplitudes and the levels of the minimum amplitudes on either side of these. These minima are clear even for the more tilted waves in the equatorial band.

Based on Figs. 1 and 2, a schematic of the observed vertical structures in both the NH part of the equatorial band and the NH band is given in Fig. 3. East of the longitude of the cyclone, there is poleward motion and ascent. Layers 1, 2, and 3 represent, respectively from the top, the layers of divergence, near-zero divergence

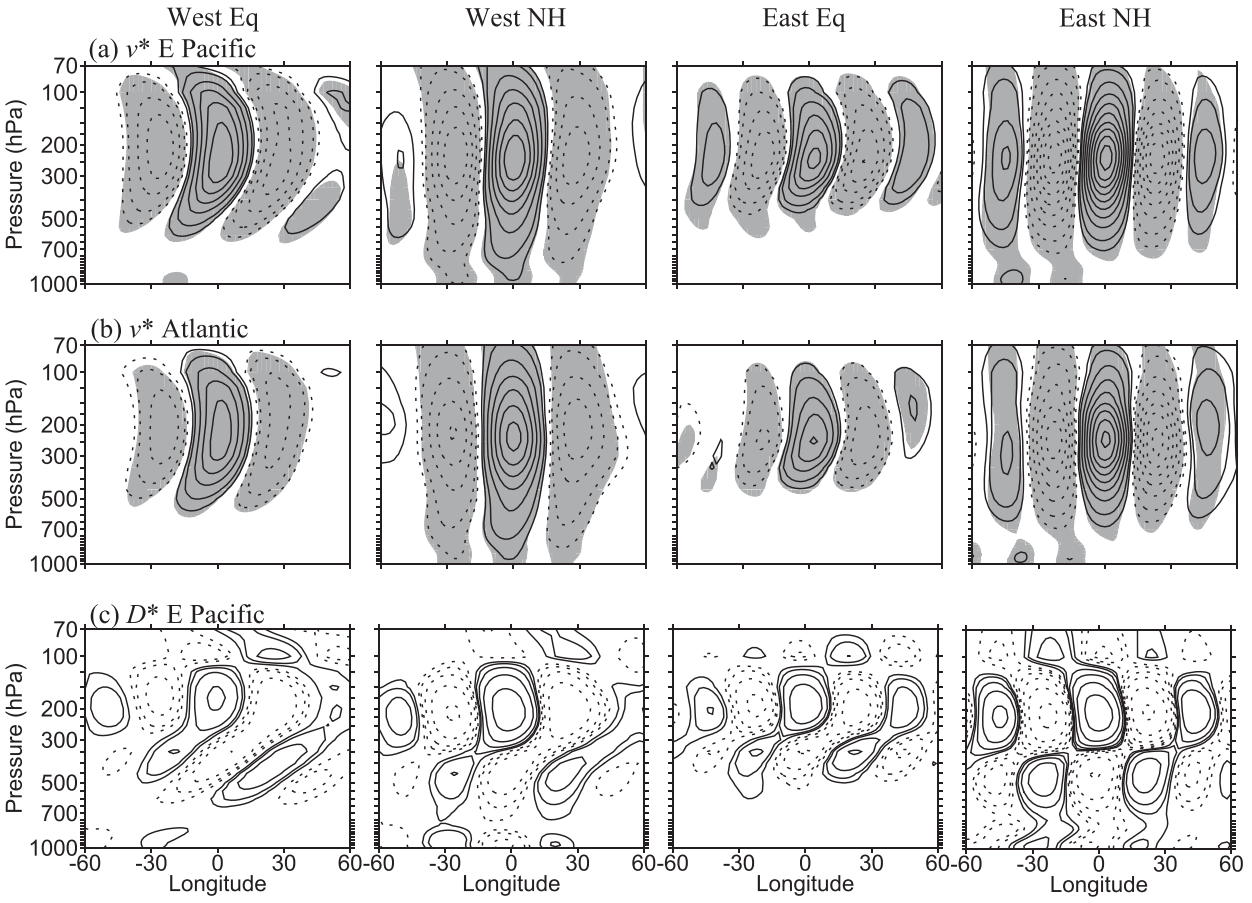

FIG. 1. (a),(b) Longitude–height cross section of meridional wind v^* (contours are ± 0.5, 1.0 m s^{-1} and then every 1 m s^{-1}) for the two latitude bands, equatorial band 10°S–10°N (Eq), and northern near-equatorial band 10°–20°N (NH), obtained by regressing v^* at each level onto the extrema of v^* at 300 hPa in that latitude band over the E. Pacific (160°–100°W) and Atlantic (50°–10°W), for (left two columns) westward-moving transients and (right two columns) eastward-moving transients. (c) As in (a), but for regressed divergence D^* (contours are ± 1, 2, 4, 8, 16, 32 $\times$ 10^{-7} s^{-1}). The shaded areas in (a) and (b) denote regions of regressed values exceeding the 95% significance level. The extremum v^* is located at 0° relative longitude with a positive value of 1.5 times its peak standard deviation in the region. Solid (dotted) contours denote positive (negative) values.

(maximum ascent), and convergence. This schematic will be used in section 5 as a basis for discussion of the vorticity budgets of the waves.

To show the horizontal structures, composites are produced for the horizontal components of velocity regressed against extrema in 300-hPa v^*. This is done for each of the cases and for layers 1 and 3. Guided by Table 1, the upper layer, layer 1, is taken to be 125–250 hPa for the equatorial band and 125–300 hPa for the NH band, and the lower layer, layer 3, is taken to be 300–500 and 400–650 hPa, respectively. The result is shown in Fig. 4. In the equatorial band the upper-layer structures are very similar to those of the WMRG wave, the eastward-moving one having a smaller wavelength, consistent with Yang and Hoskins (2016). In the lower layer, the westward-moving structure is very similar to that in the upper layer, but slightly shifted to the west and slightly bowed around the equator. The eastward-moving structure is similar to that in the upper layer, but shifted into the NH, particularly on its upstream side. The upper layers in the NH band show R1-like wave structures but only in the NH, the hemisphere containing the band and in which most of the convection occurs in the E. Pacific. Again the eastward-moving waves have a shorter wavelength. In the lower layer, these waves are similar but are tilted.

It is interesting to note that, consistent with Hoskins and Yang (2016) and Yang and Hoskins (2016), a significant part of the westward- and eastward-transient variability can be explained, respectively, by the WMRG, R1, and by the Doppler-shifted eastward-moving WMRG-E and R1-E waves. Indeed, averaged over 31 winters and in the WH upper-troposphere tropics (20°N–20°S), the WMRG and R1 waves together

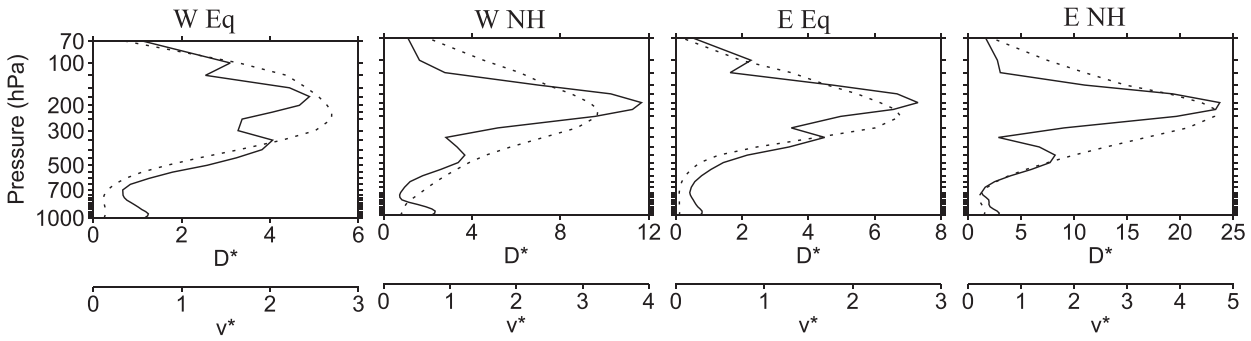

FIG. 2. Vertical profile of the E. Pacific RMS of the regressed v^* (dashed; m s^{-1}) and D^* (continuous; $\times 10^{-7}$ s^{-1}) given in Figs. 1a and 1c averaged over the longitudes shown there.

account for nearly half the variance of the westward and eastward transients. More exactly, they account for about 48% (32% for WMRG and 16% for R1) of the total westward-moving v^* variance, and WMRG-E and R1-E together take account of 42% (19% for WMRG-E and 23% for R1-E) of the total eastward-moving v^* variance.

To examine the climatology of the vertical and horizontal structures associated with the four equatorial wave modes, the regression analysis technique used to produce Fig. 1 is employed to regress the horizontal wind on to the 300-hPa equatorial wave extrema over the E. Pacific. The vertical and horizontal structures are shown in Fig. 5. The four vertical structures (Fig. 5a) are very similar to those in Fig. 1a. The amplitudes in the equatorial band (the first and third columns) are comparable to those in Fig. 1a, and those in the NH band (second and fourth columns) are about 70% of those in Fig. 1a.

The horizontal structures regressed on WMRG and WMRG-E (Figs. 5b,c, first and third column) are very similar to those for regression on the equatorial-band v^* (Fig. 4, first and third columns), indicating that the equatorial-band v^* are indeed dominated by WMRG/WMRG-E waves. However, as expected, circulations regressed onto R1/R1-E (Figs. 5b,c, second and fourth columns) show more R1-like structures than for regression onto NH-band v^* (as in Fig. 4), with NH and SH circulations generally symmetric about the equator. The exception to this is the lower-layer eastward circulation (Fig. 5c, right-hand panel). For the fields that are regressed onto NH-band v^* (Fig. 4, the second and fourth columns), the stronger v^* amplitude in the NH and weaker circulations in the SH are consistent with the convective activity and the ITCZ being in the NH. In terms of projection onto wave modes, NH v^* includes not only R1 waves but also other wave modes, such as WMRG/WMRG-E and even $n = 2$ Rossby waves. R1 waves tend to have an associated WMRG wave that is in phase in the NH and out of phase in the SH, so that the circulation is amplified in the NH but weak in the SH. Similarly R1-E waves tend to have an associated WMRG-E that is in phase in the NH. To further examine the vertical structures for the pure WMRG and R1 waves, WMRG and R1 waves have been regressed onto their v^* extrema at 300 hPa. Almost identical vertical structures to those in Fig. 5a are found (not shown).

For the analysis in the rest of this paper we will retain the use of the full v^* data. Despite this and the mixed nature of the waves in the NH band, it is convenient to often refer loosely to the waves in the four cases as WMRG, R1, WMRG-E, and R1-E, respectively.

In Figs. 1a, 1b, and 5a the vertical tilts in the westward waves in the equatorial band are consistent with them being associated with a source of WMRG waves in the upper troposphere followed by propagation upward and downward (e.g., Dunkerton and Baldwin 1995; Yang et al. 2011, 2012). The vertical tilt in the equatorial eastward wave is also in agreement with a source in the upper troposphere, and its small amplitude below 600 hPa is consistent with the lower-tropospheric easterly flow being not favorable for the existence of the

TABLE 1. Pressure levels indicating the vertical structure of RMS v^* and D^* for the westward (W)- and eastward (E)-moving waves regressed onto v^* extrema at 300 hPa for bands 10°N–10°S (Eq), and 10°–20°N (NH), for which the results are shown in Figs. 1 and 2. Given are the pressures (hPa) of RMS v^* maximum v_{max} and the upper (v_{upper}) and lower (v_{lower}) levels at which the amplitudes are about 0.1 of v_{max}; RMS divergence minima D_{min}, and maxima D_{max}.

	W Eq	W NH	E Eq	E NH
v_{upper}	70	70	100	70
v_{max}	225	225	250	225
v_{lower}	600	875	500	650
D_{min}	125	125	125	125
D_{max}	175	200	200	200
D_{min}	250–300	350	300	350
D_{max}	350	450	350	450
D_{min}	700	775	750	750

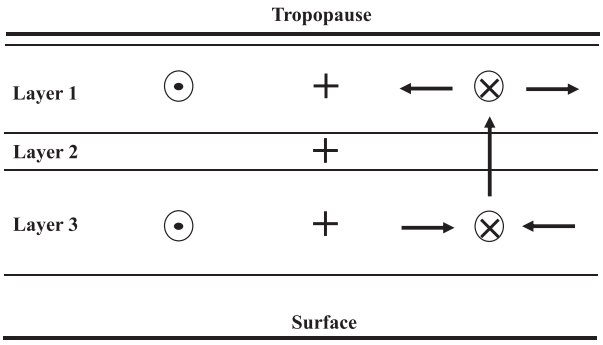

FIG. 3. Schematic height–longitude section for a sector of an equivalent barotropic wave in the NH. Cyclonic vorticity centers (+) have poleward motion (×) to the east and equatorward motion (•) to the west. In the region of poleward motion there is ascent with divergence above it (layer 1), near-zero divergence at its maximum (layer 2), and convergence below (layer 3).

Doppler-shifted eastward-moving waves (Yang and Hoskins 2016).

The dominant barotropic structure of the R1 waves in the WH is not only consistent with some previous studies (e.g., Kiladis and Wheeler 1995; Yang et al. 2007a, 2011, 2012) but also consistent with the theoretical prediction of deep structure of the R1 wave in Yang and Hoskins (2016). There it was indicated that for winter climatological-mean zonal winds and assuming the validity of the standard separation of variables, the existence of R1 waves in the WH upper troposphere requires a very large equivalent depth h. For example, h needs to be larger than 1900 m for a 15-day period (or larger than 3400 m for a 10-day period). These values are much larger than the conventional values considered for equatorial waves (e.g., Wheeler and Kiladis 1999; Kiladis et al. 2009). The large h is an indication of deep equivalent barotropic structure for the R1 wave.

4. The vorticity equation framework

In this section a scale analysis of the vorticity equation will be presented. Using typical scales for the transients shown in section 3, general implications will be drawn for the occurrence of equivalent barotropic structures in such tropical wave motions.

The vertical component of the vorticity equation, as obtained by taking the curl of the horizontal momentum equations (e.g., Hoskins and James 2014, chapter 8) may be written as follows:

$$\left(\frac{\partial}{\partial t}+\mathbf{v}\cdot\nabla\right)\zeta=-\zeta D-k\cdot\nabla\times\left(\omega\frac{\partial\mathbf{v}}{\partial p}\right)+\dot{\zeta}_F. \quad (1)$$

Here $\mathbf{v}=(u, v)$ is the horizontal velocity, $\zeta=f+\xi$ is the absolute vorticity, $\xi=\partial v/\partial x-\partial u/\partial y$ is the relative vorticity, ω is the vertical velocity in pressure coordinates, and $\dot{\zeta}_F$ is the frictional torque. The first term on the right-hand side is the stretching term and the second term includes both the vertical advection of vorticity and the twisting term.

If Eq. (1) is linearized about a zonal flow $U(y, p)$ and a wavelike perturbation moving with speed c (relative to the ground) is considered, then it becomes

$$\underbrace{(U-c)\frac{\partial\xi}{\partial x}}_{\text{ZA: }\frac{UV}{L^2}}+\underbrace{\beta^*v}_{\text{MA: }\beta V}=\underbrace{-f^*D}_{\text{ST: }f\frac{W}{H}}+\underbrace{\frac{\partial}{\partial y}\left(\omega\frac{\partial U}{\partial p}\right)}_{\text{VAT: }\frac{WU}{LH}}+\underbrace{\dot{\zeta}_F}_{\text{FT: }\frac{1}{\tau_F}\frac{V}{L}}. \quad (2)$$

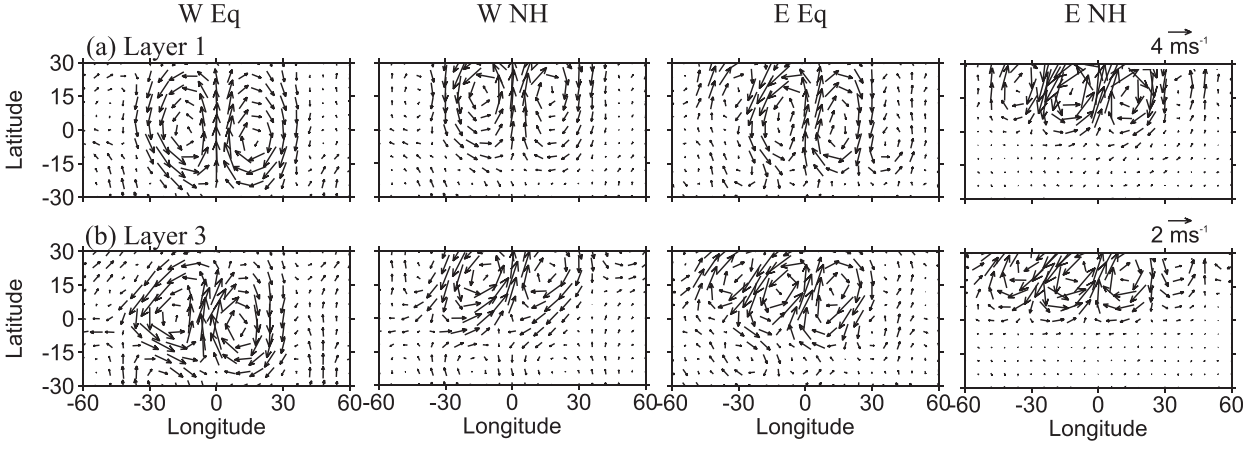

FIG. 4. Horizontal winds on (a) upper layer (layer 1: 125–250 hPa for the equatorial band and 125–300 hPa for the NH band) and (b) lower layer (layer 3: 300–500 hPa for the equatorial band and 400–650 hPa for NH band), regressed onto v^* extrema at 300 hPa for the equatorial and NH bands and for westward- and eastward-moving components in the E. Pacific.

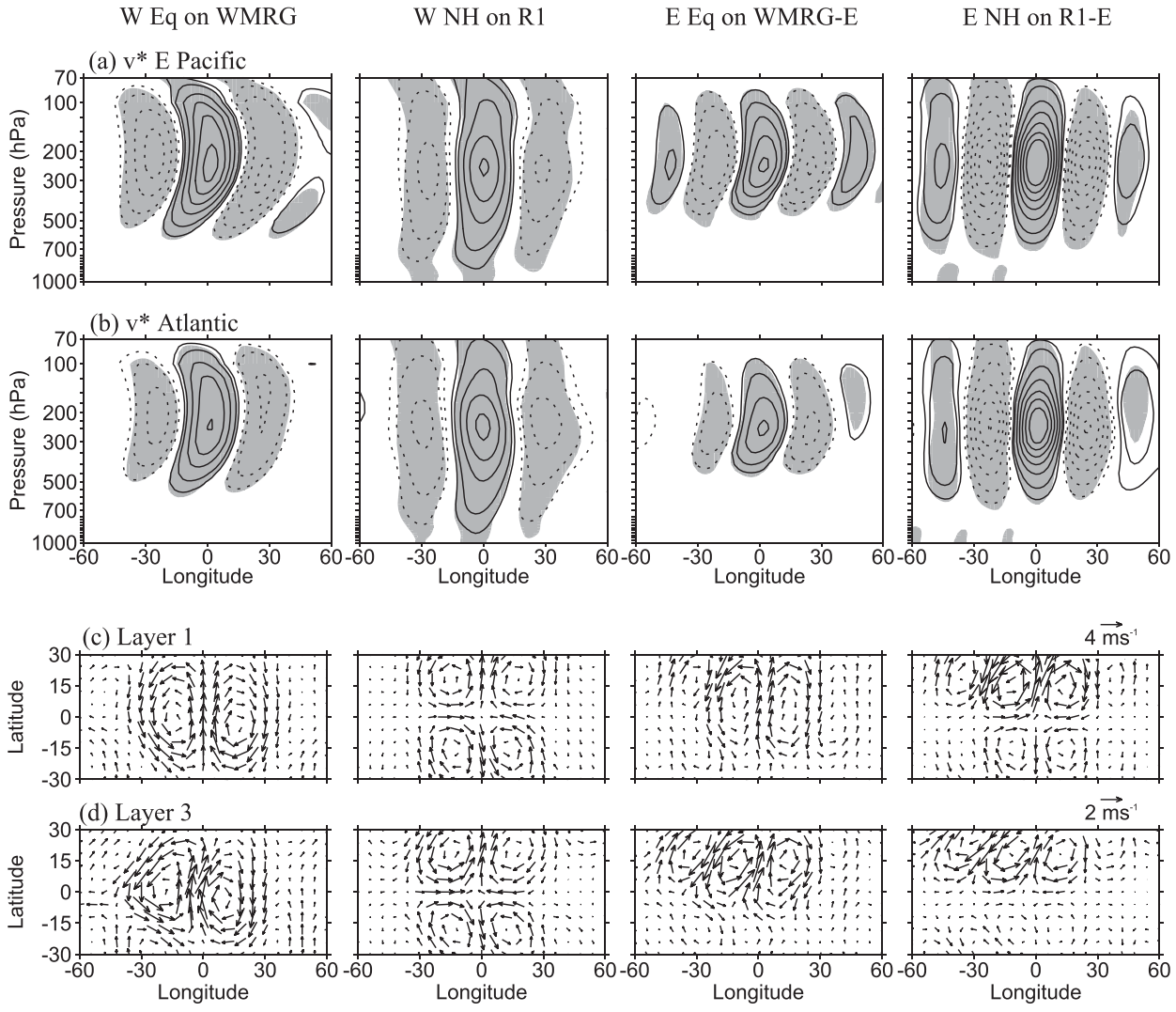

FIG. 5. Results for the E. Pacific for regressions onto the extrema of WMRG/WMRG-E and R1 and R1-E at 300 hPa. (a) Longitude–height cross section of meridional wind v^* as in Fig. 1a. (c),(d) Horizontal winds at layers 1 and 3 as in Fig. 4.

In Eq. (2), the first term on the left-hand side (lhs), herein denoted "ZA," is the zonal advection relative to the wave of perturbation vorticity ξ. The second term on the lhs, denoted "MA," is the meridional advection of the mean-state absolute vorticity, $f^* = f - \partial U/\partial y$, with $\beta^* = df^*/dy$. The first term on the rhs is the stretching by the perturbation vertical velocity and its associated divergence, denoted "ST." The second term on the rhs is the vertical advection and twisting term, denoted "VAT." The final term is the frictional torque, denoted "FT."

Under each term in Eq. (2), typical scales are given. In these, U, V, and L are typical values of $U - c$, v, and a horizontal length scale, respectively. Hence ξ scales as V/L. As indicated, to scale the first two terms on the rhs it is convenient to use corresponding height coordinate versions and typical height and vertical velocity scales H and W.

We now consider the likely relative magnitudes of the terms in the vorticity equation for the observed waves in the E. Pacific and Atlantic. The relative scales of the two terms on the lhs are

$$\mathrm{MA/ZA} \sim \beta L^2/U.$$

Taking $U \sim 10\,\mathrm{m\,s^{-1}}$, $L \sim 0.7 \times 10^6\,\mathrm{m}$ (a total wavenumber 9), and $\beta = 2.3 \times 10^{-11}\,\mathrm{m^{-1}\,s^{-1}}$ (a typical value below 20° of latitude) gives $\beta L^2/U \sim 1$. An equivalent statement is that the horizontal scale L is of order the Rhines scale, $(U/\beta)^{1/2}$. This scaling corresponds to one of the regimes discussed by Yano and Bonazzola (2009). The comparability of the scales for ZA and MA is

characteristic of equivalent barotropic behavior, with large cancellation expected between the two terms.

The ratio of the first two terms on the rhs is

$$\mathrm{VAT/ST} \sim U/fL.$$

This Rossby number would usually be taken to be small in the extratropics. However, in the tropics in regions with significant shear in the zonal wind this is not necessarily the case. Taking the above scales for U and L and also $f \sim 0.25 \times 10^{-4}$ (latitude $\sim 10°$) gives $U/fL \sim 1/1.8$. Therefore for these scales in the near-equatorial region the VAT term can be expected to comparable to, or somewhat smaller than, the stretching term.

The ratio of the typical magnitude of the ST term to those of the individual terms on the lhs depends on a scaling for W/H. If this scaling is derived from balancing horizontal and vertical advection in the thermodynamic equation, then some manipulation (e.g., Hoskins and James 2014, sections 12.3 and 12.4) gives

$$\mathrm{ST/ZA} \sim f^2L^2/N^2H^2,$$

where N is the buoyancy frequency. Taking $N \sim 1 \times 10^{-2}\,\mathrm{s}^{-1}$ and $H \sim 5\,\mathrm{km}$ (so that $\pi H \sim$ tropopause height) gives

$$\mathrm{ST/ZA} \sim 3/25 \sim 1/8.$$

The smallness of this ratio is consistent with the analysis of Charney (1963) for larger vertical scales in the tropics, and his statement that, to first order, the barotropic vorticity equation is applicable at every level. However, in this paper the importance of the smaller ST term for enabling the vertical structure will be demonstrated. If the balance in the thermodynamic equation is instead mainly between convective heating and adiabatic cooling, then W, and hence the ratio ST/ZA, could be larger than the above estimate.

Finally, the scale of the frictional torque compared with the zonal advection is

$$\mathrm{FT/ZA} \sim \frac{L/U}{\tau_F}.$$

The advection time scale $L/U \sim 0.7 \times 10^5\,\mathrm{s} \sim 1$ day, and so the relative magnitude of the frictional torque depends on its time scale compared with 1 day. Any cumulus friction is likely to act on the longer time scales than this. However, a 1-week time scale could make the frictional torque comparable to the stretching term.

Guided by the observed wave structure in Figs. 1, 2, and 4 and by the above scale analysis, we define an equivalent barotropic structure to be one in which

1) the wind field shows only small tilt with height,
2) the ZA and MA terms dominate the vorticity equation with a large cancellation between them,
3) the residual of the ZA and MA terms has opposite signs in the upper troposphere and the mid-/lower troposphere, and
4) the ST term acts in the sense of balancing this residual in both regions.

In this light we consider the idealized NH equivalent barotropic perturbation sketched in Fig. 3 and the vorticity budget for the region of poleward motion ahead of the cyclonic region. In layer 1 in the region above the maximum ascent, there will be divergence and vortex shrinking, that is, ST negative. In this region the negative ZA outweighs the positive MA, and so the negative ST is in the sense of balancing their sum. In layer 3, below the ascent maximum, there is convergence and vortex stretching, ST positive. Here, the positive MA dominates the negative ZA, and the positive ST acts in the sense of balancing their sum.

In layer 2, where ST is negligible, Eq. (2) gives

$$(U_2 - c)\frac{\partial \xi_2}{\partial x} + \beta_2^* v_2 = R_2. \tag{3}$$

Here R_2 is the sum of VAT and FT at this level, and will be assumed for the moment to be negligible compared with the other terms. Because the observed waves are predominantly rotational, we can define a horizontal length scale L derived from basic fields by $L^2 = -v/(\partial\xi/\partial x)$.

This would give $L = 1/K$ for a harmonic wave of total wavenumber K. Then Eq. (3) gives

$$U_2 - c = \beta_2^* L^2. \tag{4}$$

Therefore the intrinsic phase speed, $c - U$, is negative (westward) and is proportional to the square of the horizontal length scale, as in the general scale analysis above.

For layers 1 and 3 it is also assumed for the moment that $R = \mathrm{VAT} + \mathrm{FT}$ is negligible. Then Eq. (2) gives

$$(U_1 - c)\frac{\partial \xi_1}{\partial x} + \beta_1^* v_1 = -f_1^* D_1 < 0 \quad \text{and}$$

$$(U_3 - c)\frac{\partial \xi_3}{\partial x} + \beta_3^* v_3 = -f_3^* D_3 > 0.$$

In terms of the horizontal scale L, this implies

$$U_1 - c - \beta_1^* L_1^2 > 0 \quad \text{and} \tag{5}$$

$$U_3 - c - \beta_3^* L_3^2 < 0. \tag{6}$$

Assuming that the vertical variation of c, β^*, and L is not significant, Eqs. (5) and (6) together with Eq. (4) are consistent with $U_1 > U_2 > U_3$—that is, a westerly shear with height. As well as being satisfied in middle latitudes, this condition is satisfied in the tropical E. Pacific and Atlantic, particularly in boreal winter. Therefore, in these regions and in this season, the observed equivalent barotropic behavior of waves moving westward relative to the wind is consistent with this discussion.

It was noted above that Eq. (4) [and also Eq. (5)] indicates that the wave must have an intrinsic westward phase speed that is negative. Equation (6) for the wave in the lower layer could be satisfied with an intrinsic phase speed that is westward or eastward. However, in reality the wave will tend to be confined above a critical layer at which the intrinsic phase speed would become zero, so that the intrinsic phase speed is westward at all levels of significant amplitude.

A similar discussion, but with descent to the east of the cyclonic vorticity, would be consistent with a barotropic structure in an easterly sheared basic flow. In this case, the large westward intrinsic phase speed would be in the lower layer. Nevertheless, although the easterly shear does exist in the EH, we are not aware of any evidence that such equivalent barotropic waves with descent to the east of cyclone are observed to occur there.

In the next section the dynamics of the observed waves will be analyzed in the context of the general discussion given in this section.

5. Discussion of the observed waves and terms in their vorticity budget

a. *Wave characteristics*

Figure 6 gives vertical profile information on the ambient zonal winds U and the phase speeds c in the E. Pacific for the equatorial and NH bands, as determined from the observational data for the 31 winters. The value of c at each level is obtained from regressed v^* fields in a domain from $-60°$ to $+60°$ longitude and for lags from day -6 to $+6$. In such longitude–time diagrams, phase speed is often simply estimated from a slope line on the plot. However, here a more objective way, the Radon transform method, is used. This method can objectively compute the direction of travel of the wave in the longitude–time domain and, thus, its phase speed. The method was first described by Radon (1917) and has been applied in studies of oceanic planetary waves (e.g., Challenor et al. 2001) and atmospheric waves (Yang et al. 2007b). A brief introduction to this method and an example of its application is given in the appendix of Yang et al. (2007b).

It is seen that despite the large vertical shear of U, c for each wave does not change much in the vertical, indicating their strong vertical coupling. Only westward-moving waves in the equatorial band exhibit any significant change in c with height, it being larger in the lower troposphere and above 100 hPa than in the middle to upper troposphere. This is consistent with the waves with faster phase speed being able to more easily propagate vertically into these regions from the source region in the upper troposphere (e.g., Yang et al. 2011, 2012).

For the westward-moving waves (negative c) in both latitude bands, $U - c$ is clearly positive throughout. However, because of the strong westerly shear of the zonal wind, $U - c$ is much larger in the upper than in the lower troposphere.

Eastward-moving waves in both latitude bands have very similar positive c and for them $U - c$ is also positive in the upper troposphere, indicating westward intrinsic phase speeds. There do appear to be critical levels near 350 hPa for the equatorial band and 400 hPa for the NH band at which $U - c = 0$. Despite this, the two waves are seen to have significant magnitudes below this. This can be explained by the fact that the tropical zonal wind has large ENSO-related interannual variability in the E. Pacific (e.g., Yang and Hoskins 2013; Yang and Hoskins 2016), as well as shorter time scale variability as discussed in Yang and Hoskins (2016). To show the possible importance of this shorter-time-scale variability, the standard deviations of 30-day-average U departures from the seasonal mean across the E. Pacific are calculated, assuming that this time scale can be considered to be the ambient zonal flow on which the waves propagate. This is done for both the equatorial and NH bands. Averaged over the years, this standard deviation in the upper troposphere is found to be 48% and 32% of the mean in the equatorial and NH bands, respectively. The range of one standard deviation of U (USD) is shown in Figs. 6a and 6c by two thin solid lines. Taking the zonal flow as U plus one standard deviation (U + USD) would take the critical levels for the eastward-moving waves down to near 400 hPa for the equatorial band and 550 hPa for the NH band, which is much more consistent with the observed structures.

It is of interest to investigate the extent to which Eq. (4) is satisfied and the manner in which this is achieved near the level of zero divergence (layer 2). Table 2 shows values taken from observed fields and compares the horizontal length scale calculated from Eq. (4) with that observed. For the westward-moving waves at both latitude bands, there is good agreement. For the eastward-moving waves, two values of the zonal flow are used. The first is the average value for that layer. However, this

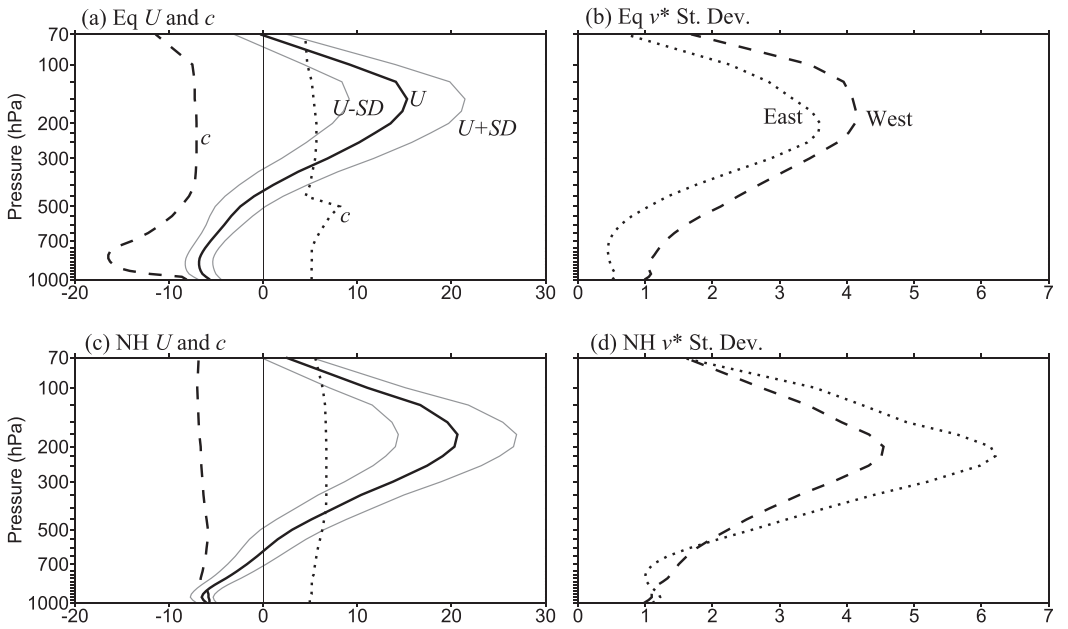

FIG. 6. Vertical profiles of (a) tropical zonal wind U (solid; m s^{-1}) for the equatorial band, U plus and minus one 30-day standard deviation (USD, thin solid; m s^{-1}), and phase speed c (m s^{-1}) for westward- (dashed) and eastward-moving (dotted) v^* for the equatorial band in the E. Pacific; (b) standard deviations of westward- (dashed) and eastward-moving (dotted) v^* for the equatorial band in the E. Pacific. (c),(d) As in (a) and (b), respectively, but for the NH band. Negative (positive) c indicates westward (eastward) moving.

leads to a length scale considerably smaller than that observed. The second, recognizing the likelihood of these waves occurring in the periods with stronger westerlies, uses U + USD. In both cases this yields a length scale more comparable to that observed, so that the observed scale is again found to be a consistent fit with such an ambient zonal flow stronger than the climatological average.

b. *Detailed analysis of the vorticity equation for the observed waves*

In this subsection, the vorticity equation is diagnosed in detail for each wave and for layers 1 and 3. There is no attempt here to close the vorticity budget, which in general remains a problem in the equatorial region. As the vorticity equation terms will be determined for regressed rather than actual instantaneous fields, a closed budget would not be expected in any case. Therefore it is considered that attempting to determine VAT and FT would add unnecessary complexity to the present discussion of the equivalent barotropic structure of the waves. However, we are looking for the general satisfaction of the equivalent barotropic conditions given in section 4, and based on the scale analysis there, it is expected that the residual R in the balance of ZA + MA by ST, would have a magnitude generally comparable with and not much larger than that of ST itself.

To diagnose the terms in the vorticity equation associated with the waves, the wind components u^* and v^* at each grid point and at each level are separately regressed onto the 300-hPa v^* extrema. This is done separately for each latitude band and for westward- and eastward-moving waves. Then the relative vorticity and the divergence and the terms in the vorticity equation are calculated from the regressed (u^*, v^*) using finite differences.

TABLE 2. Horizontal wave scales L_{calc} ($\times 10^6$ m) determined by calculation from the simplified vorticity equation at the level of maximum vertical motion, Eq. (4), compared with observed horizontal scales L_{obs}. The mean zonal flow U, standard deviation of 30-day-mean U (USD), and phase speeds c are given for the regressed waves in v^* for the latitude bands 10°N–10°S (Eq) and 10°–20°N (NH), at layer 2 (250–300 hPa for Eq and 300–400 hPa for NH), and for westward (W)- and eastward (E)-moving waves. Values of $U - c$ and L_{calc} are determined from these, and for the eastward waves values using U + USD are given in parentheses. Wavenumbers k and l are estimated observed zonal and equivalent meridional wavenumbers, and $L_{obs} = a/(k^2 + l^2)^{1/2}$, where a is the radius of Earth. The unit for the speeds is m s^{-1}.

	U	USD	c	$U - c$	L_{calc}	k	l	L_{obs}
W Eq	8.5	5.2	−7.1	15.6	0.89	6	3, 4	0.92
W NH	10.6	4.6	−6.3	16.9	0.83	6, 7	4	0.83
E Eq	8.5	5.2	5.6	2.9 (8.2)	0.39 (0.64)	7, 8	4	0.75
E NH	10.6	4.6	6.7	3.9 (8.5)	0.40 (0.60)	7, 8	6	0.66

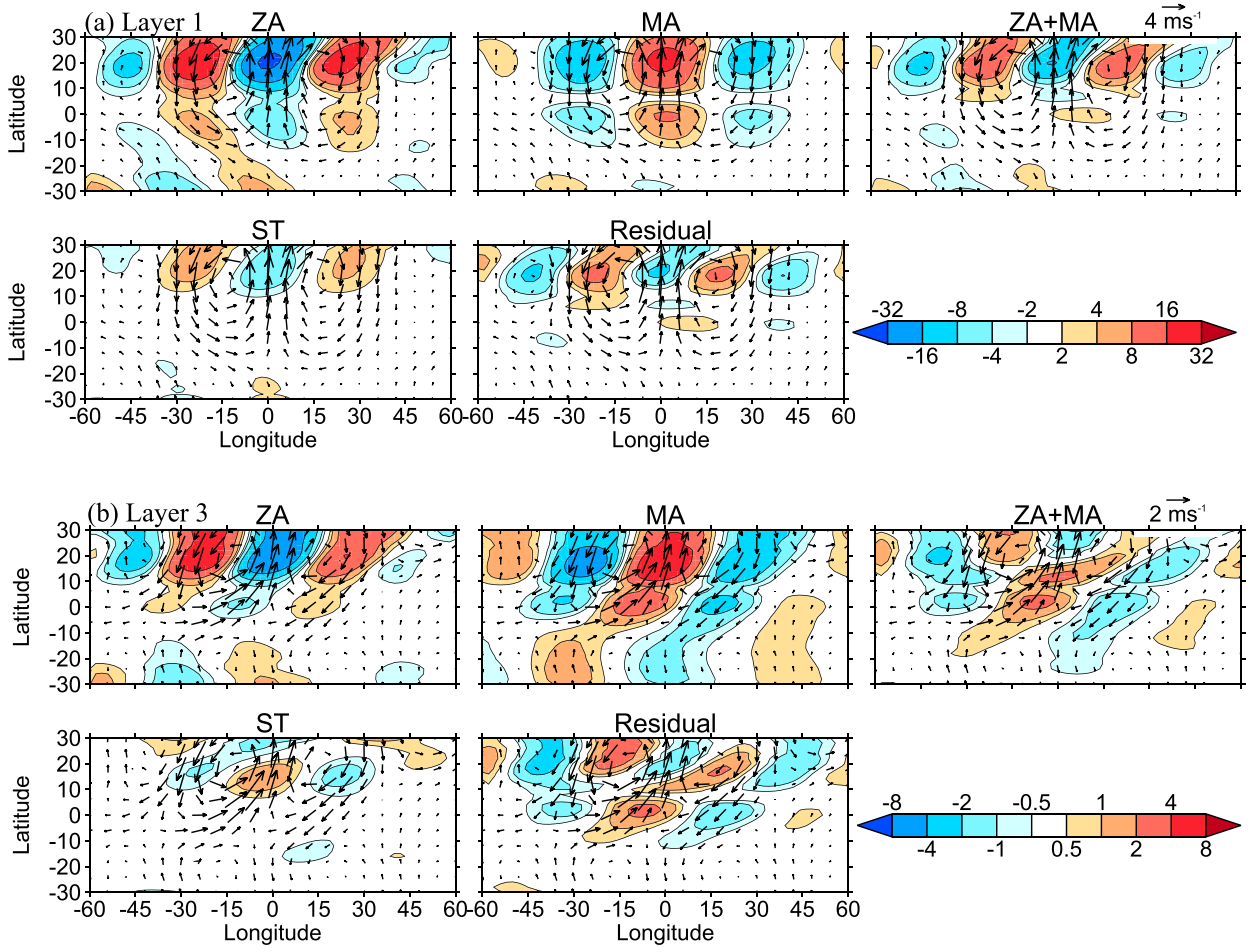

FIG. 7. Horizontal distribution of vorticity equation terms (colored contours; $10^{-11}\,s^{-2}$) and (u^*, v^*) (vectors) in (a) layer 1 and (b) layer 3, calculated from the westward-moving (u^*, v^*) regressed onto the extrema of westward-moving v^* at 300 hPa at NH band in the E. Pacific, and averaged for 31 winters. The extrema in v^* are located at 0° relative longitude with positive value 1.5 times its peak standard deviation in the region.

As an example, for the westward-moving waves regressed onto the NH band v^*, Fig. 7 shows vorticity equation terms averaged over each of layers 1 and 3, corresponding to the upper and lower layers in Fig. 4. From left to right are shown ZA, MA, ZA + MA, ST, and the residual (R = ZA + MA − ST).

Near 0° longitude where $v^* > 0$, the budget is consistent with the earlier qualitative discussion. There, ZA

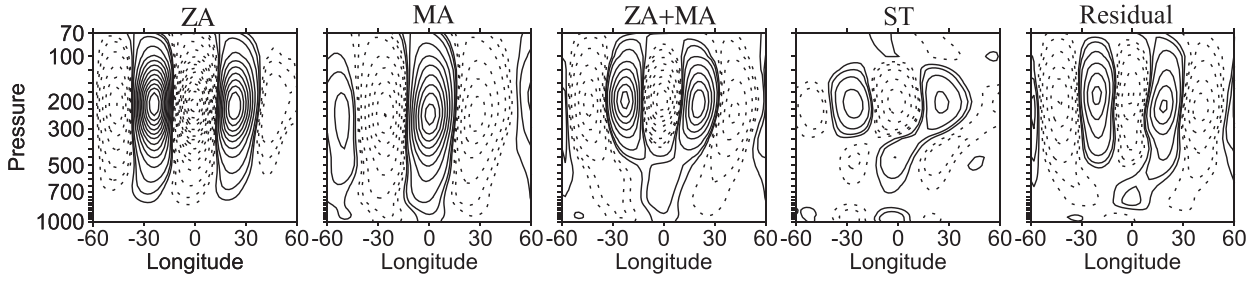

FIG. 8. Zonal–vertical distribution of vorticity equation terms (contours are ±0.5, 1, 2 × $10^{-11}\,s^{-2}$ and then every 2 × $10^{-11}\,s^{-2}$) for westward-moving waves in the NH band over the E. Pacific. The extrema in v^* are located at 0° relative longitude with a positive value of 1.5 times its peak standard deviation in the E. Pacific.

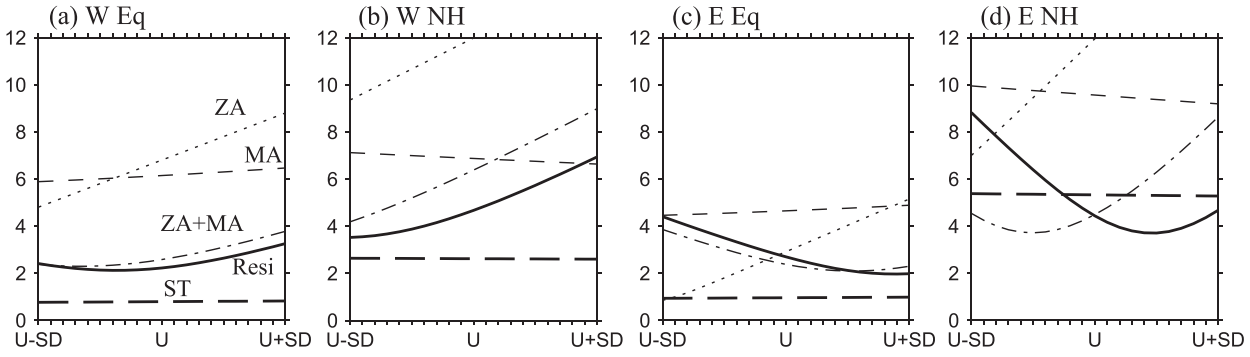

FIG. 9. Amplitudes (RMS) of the five vorticity equation terms ($\times 10^{-11}$ s^{-2}) as a function of ambient zonal flow U varying between plus and minus one standard deviation in layer 1 for (a),(b) westward and (c),(d) eastward components. The RMS amplitudes are calculated from −60° to +60° relative longitudes.

is negative while MA is positive. In the upper layer ZA is larger than MA while in the lower layer it is smaller equatorward of 20°N. As a result of the partial cancellation between them, the magnitude of the total horizontal advection ZA + MA is smaller and it has opposite signs in the two layers at 0°–20°N. The ST term is generally similar in structure to that of ZA + MA, particularly in layer 1, and also shows similar opposite signs in the upper and lower troposphere. It therefore acts to balance the vorticity budget. However the amplitudes are such that the balance is not complete, and the residual term R does indeed have an amplitude comparable to that of ST.

To indicate the vorticity budget at all levels in the troposphere for 10°–20°N westward-moving waves, the zonal–vertical distribution of the same five vorticity budget terms averaged over the relevant latitude band is shown in Fig. 8. As anticipated, ZA and MA have opposite signs throughout the troposphere, with the former dominating in their sum above 400 hPa and the latter dominating below this. The behavior of ST is similar but R generally looks like a weakened version of ZA. Therefore a smaller R would be achieved using a slightly weaker zonal flow.

Given that the ambient zonal flow has large variability, it is appropriate to consider the use for each wave of a best-fit zonal flow that minimizes the residual term in the vorticity equation for that wave. Figure 9 shows for both latitude bands and westward- and eastward-moving waves the amplitudes (RMS) of the five vorticity budget terms in the upper layer (layer 1) and the residual for the zonal flow varying between U − USD and U + USD in layer 1. As expected, only the ZA (dotted) has significant variation with U. The very small variation in MA (dashed) is because of variation in the flow curvature term in β^*. The region with ZA > MA indicates the zonal flow range for a barotropic structure to occur, while ZA < MA indicates a baroclinic structure. ZA + MA (dashed–dotted) also has variation with U, and ST (long dashed) is nearly a constant because $-U_y$ variation is very small compared to f. The residual (solid) has a minimum in all cases at a value of U which can be considered to be a best-fit wind, $U_b = U + \Delta U$, where $\Delta U = \alpha$USD. It is notable that for the westward-moving waves U_b tends to appear at a smaller value than the climatological U, with $\alpha = -0.4$ for the equatorial band and −1.1 for the NH band, whereas for the eastward-moving waves, U_b occurs at a larger value than U, with $\alpha = +0.9$ and +0.5, respectively. This is again consistent with the idea that westward-moving R1 waves can only exist in westerlies that are not too strong and that Doppler-shifted eastward-moving WMRG-E and R1-E waves, and especially the former, can only exist in strong westerlies. In all cases, the best-fit wind falls in the range of potential barotropic structure (ZA > MA), consistent with the dominant equivalent barotropic structure of the waves (Fig. 1). The values of U, USD, α, and best-fit ΔU

TABLE 3. Mean zonal flow U, its standard deviation (USD), and the associated best-fit zonal wind ($U + \Delta U$, with $\Delta U = \alpha$USD), chosen to give the smallest vorticity budget residual amplitude for the regressed waves in the latitude bands 10°N–10°S (Eq) and 10°–20°N (NH) and three layers for westward (W)- and eastward (E)-moving waves. Layer 1 is 125–250 hPa for Eq and 125–300 hPa for NH. Layer 2 is 250–300 hPa for Eq and 300–400 hPa for NH, and layer 3 is 300–500 hPa for Eq and 400–650 hPa for NH.

			W		E	
Lat: Layer	U	USD	α	ΔU	α	ΔU
Eq: 1	13.3	6.0	−0.4	−2.4	0.9	5.4
Eq: 2	8.5	5.2	−0.2	−1.0	1.4	7.3
Eq: 3	1.7	3.7	0.2	0.7	1.8	6.6
NH: 1	18.2	5.8	−1.1	−6.4	0.5	2.9
NH: 2	10.5	4.6	−0.8	−3.7	0.9	4.1
NH: 3	2.8	3.2	−0.7	−2.2	1.0	3.2

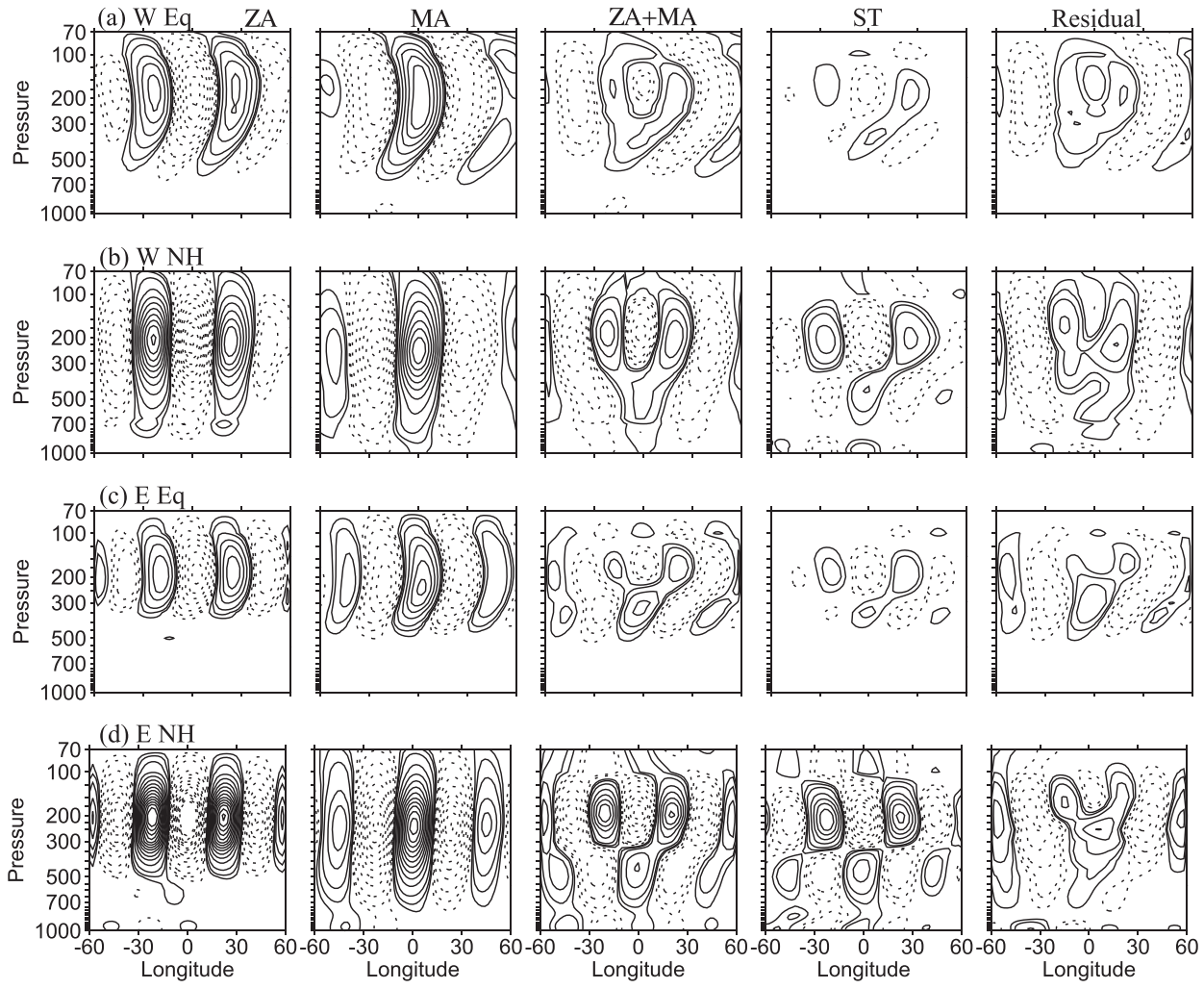

FIG. 10. Zonal–vertical distributions of vorticity equation terms as in Fig. 8 but calculated for all cases and using the best-fit U: (a),(b) westward- and (c),(d) eastward-moving components. The amplitudes are calculated from −60° to +60° relative longitudes.

for the four waves are given in Table 3. For completeness the best-fit values in layers 2 and 3 are also shown. A best fit is found within the range $U \pm$ USD except for the eastward-moving equatorial band in layers 2 and 3. These best-fit winds (with α being capped at 1) will be used in the following vorticity budget analysis.

The amplitudes for levels below layer 3 to 850 hPa (not shown) demonstrate little variation in any term with the zonal flow used. In all cases ZA < MA and there is no clear best-fit zonal wind.

The zonal–vertical distribution of the vorticity budget terms for the four cases and using the best-fit zonal winds is shown in Fig. 10. Comparison of the NH westward case (Fig. 10b) with Fig. 8 confirms that the smaller U values in ZA do lead to a reduced residual, R. The waves all show simple structures with cancelling ZA and MA but with the former dominant above about 250–300 hPa and the latter below this. In each case, the ST term is generally in the sense of balancing ZA + MA, though R is generally comparable with it, as anticipated.

To quantify the relationship of vorticity budget terms, the two correlations, ZA with MA and ZA + MA with ST, have been calculated at each level. The correlations between ZA and MA are very strongly negative (greater than 0.9 compared with a 95% significance level of 0.31) throughout the troposphere for the westward NH band. The highly significant negative correlations also exist at all levels above 750 hPa for the westward equatorial band and above 500–550 hPa for both eastward-moving waves. The correlations between ZA + MA and ST are positive and very significant in the upper and lower layers in all cases, with values varying from 0.4 to 0.99.

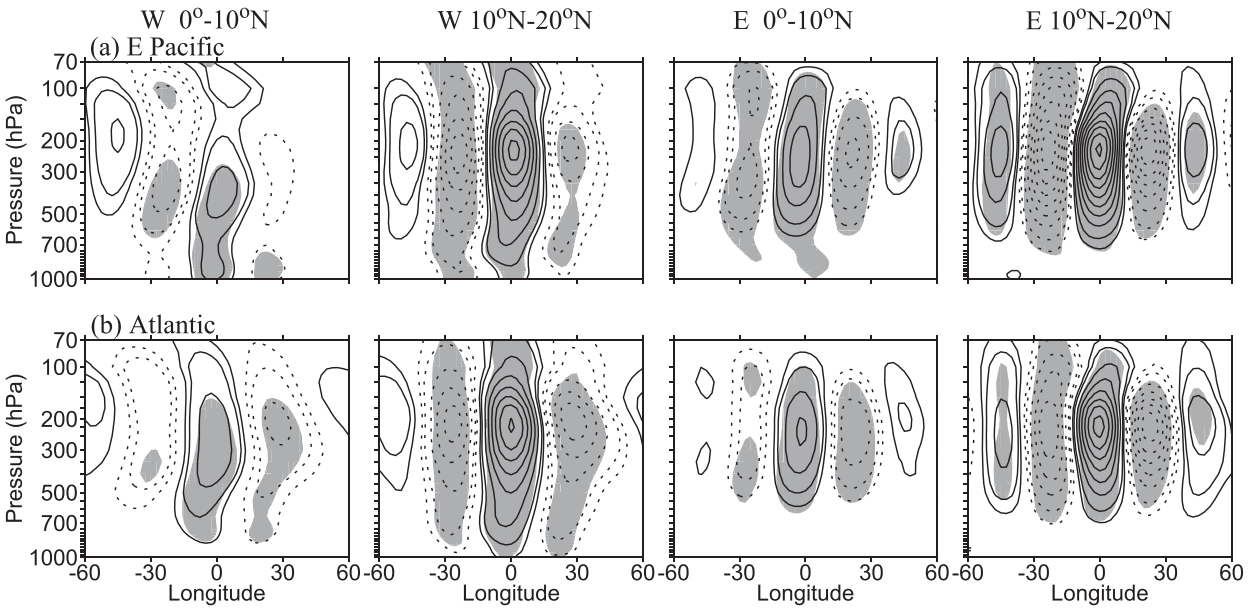

FIG. 11. As in Figs. 1a and 1b, but for waves connected to tropical convection, obtained by regressing v^* in the 0°–10° and 10°–20°N bands onto the extrema of (left two columns) westward OLR* component and (right two columns) eastward OLR* component at 0°–20°N over (a) E. Pacific and (b) Atlantic. The extrema of OLR are located at 0° relative longitude with a negative value of 1.5 times its peak standard deviation in the region. Solid (dotted) contours denote positive (negative) winds. Other conventions are as in Fig. 1.

6. Summary and discussion

The analysis of ERA-Interim data in the period 1979–2010 presented here gives strong evidence that for the climatological-mean boreal winter, the WH equatorial and NH near-equatorial, westward-, and eastward-moving transients have structures that are predominantly equivalent barotropic in the vertical and wavelike in the zonal direction. The westward- and eastward-moving waves in the equatorial region have strong projections onto the WMRG and the Doppler-shifted WMRG-E waves, respectively, with amplitudes mainly in the upper troposphere. The vertical tilts that are present are consistent with propagation upward and downward from an upper-tropospheric source. The westward-moving waves in the NH near-equatorial region have strong projections onto the R1 wave as well as the WMRG wave, consistent with the activity mainly occurring in the NH. Similarly the eastward-moving waves there have strong projections onto the Doppler-shifted R1-E wave as well as the WMRG-E. The equivalent barotropic nature of the NH near-equatorial waves is even clearer, and their amplitude extends into the lower troposphere.

Since many equatorial waves are closely connected to tropical convection (e.g., Wheeler and Kiladis 1999; Yang et al. 2007a,b,c), it is of interest to investigate the vertical structure of transients that are directly connected to convection. Figure 11 shows the result of regressing westward and eastward v^* in the two latitude bands, 0°–10° and 10°–20°N, onto the extrema of westward-moving OLR* in the NH tropical region (0°–20°N) in the E. Pacific and Atlantic. These latitude bands for OLR are used as they contain most of the OLR variance in the E. Pacific. The wavelike barotropic structures are generally very similar to those shown in Figs. 1a and 1b, which were derived from regression against v^* at 300 hPa in their own latitude bands. This is particularly the case for the transients in the NH band. The convectively connected waves in the near-equatorial band 0°–10°N are relatively weaker but still very similar in structure. A similar regression has also been performed for the WMRG, R1, WMRG-E, and R1-E waves, with very similar results (not shown). It is found that the ascent in the waves in the reanalysis data is generally quite consistent with the independent OLR data and that it occurs in the locations at which equatorial wave theory would suggest lower-level convergence.

The main focus of this paper has been on how barotropic vertical structures are possible in the tropics, using analyses of the balance of terms in the vorticity equation. As summarized in Figs. 12a and 12b and discussed in the introduction, the basis for the predominant conceptual model for the tropics in recent decades is that ascent gives divergence and an anticyclonic vorticity tendency in the upper troposphere and convergence and cyclonic vorticity tendency below it (Fig. 12a).

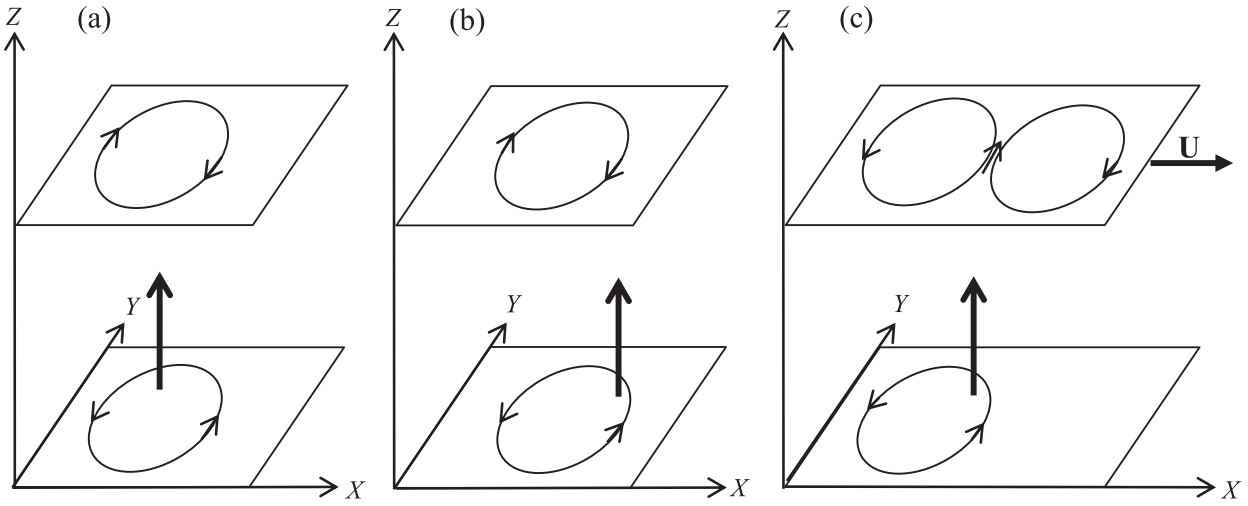

FIG. 12. Schematic diagram of the formation of baroclinic and barotropic structures in the NH tropics. (a) Deep convective heating is balanced by adiabatic cooling associated with ascent. Divergence above the maximum ascent gives an anticyclonic vorticity tendency there, and convergence below gives a cyclonic vorticity tendency there. (b) The β effect leads to a westward drift both above the heating maximum and below it. A steady situation is reached when the upper equatorward motion and the lower poleward motion are in the longitude of the ascent, giving a baroclinic structure in the vertical. (c) In the presence of strong westerly shear and upper-tropospheric westerly winds relative to the motion of the convection, zonal advection can dominate the β effect there and lead to eastward displacement of the upper wave. If the β effect still dominates for the lower wave, the resulting structure is equivalent barotropic.

Relative to the ascent (that may be moving), the β effect causes a westward drift. This leads to a balance between the meridional advection of planetary vorticity, the β term, and the vortex shrinking above and vortex stretching below when the upper anticyclone and lower cyclone are to the west (Fig. 12b). The upper flow is then toward the equator and the lower flow away from it—the classic first-baroclinic-mode structure for the tropics. However, in the WH the westerly shear is so strong that the usually neglected zonal vorticity advection by the upper-tropospheric westerlies dominates over the β term. In this case, as illustrated in Fig. 12c, in the balanced state in the upper troposphere the anticyclone is to the east and the flow in the region of the ascent is now away from the equator. In the lower region the β term dominates as before, and so the vertical structure is now equivalent barotropic. As hypothesized by Charney (1963), to a first approximation for deep waves the barotropic vorticity equation is applicable at every level. However, the smaller vortex stretching/shrinking term associated with ascent and descent enables vertical coherence with the observed equivalent barotropic structure. This picture is familiar for the extratropics. However its relevance to the transient motions near the equator is thought to be novel and to contribute to the fundamental understanding of tropical waves.

Acknowledgments. We thank the very helpful comments of Matt Wheeler and two anonymous referees on the original version of this paper. GYY acknowledges the support of the National Centre for Atmospheric Science (NCAS) and the NERC project (NE/I012419/1). GYY is a member of NCAS.

REFERENCES

Challenor, P. G., P. Cipollini, and D. Cromwell, 2001: Use of the 3D radon transform to examine properties of oceanic Rossby waves. *J. Atmos. Oceanic Technol.*, **18**, 1558–1566, doi:10.1175/1520-0426(2001)018<1558:UOTRTT>2.0.CO;2.

Charney, J. G., 1963: A note on large-scale motions in the tropics. *J. Atmos. Sci.*, **20**, 607–609, doi:10.1175/1520-0469(1963)020<0607:ANOLSM>2.0.CO;2.

Dee, D. P., and Coauthors, 2011: The ERA-Interim reanalysis: Configuration and performance of the data assimilation system. *Quart. J. Roy. Meteor. Soc.*, **137**, 553–597, doi:10.1002/qj.828.

Dunkerton, T. J., and M. P. Baldwin, 1995: Observation of 3–6-day meridional wind oscillations over the tropical Pacific, 1973–1992: Horizontal structure and propagation. *J. Atmos. Sci.*, **52**, 1585–1601, doi:10.1175/1520-0469(1995)052<1585:OODMWO>2.0.CO;2.

Gill, A. E., 1980: Some simple solutions for heat induced tropical circulations. *Quart. J. Roy. Meteor. Soc.*, **106**, 447–462, doi:10.1002/qj.49710644905.

Holton, J. R., 1969: A note on the scale analysis of tropical motions. *J. Atmos. Sci.*, **26**, 770–771, doi:10.1175/1520-0469(1969)026<0770:ANOTSA>2.0.CO;2.

Hoskins, B. J., and I. N. James, 2014: *Fluid Dynamics of the Mid-latitude Atmosphere.* Wiley, 408 pp.

——, and G.-Y. Yang, 2016: The longitudinal variation of equatorial waves due to propagation on a zonal varying flow. *J. Atmos. Sci.*, **73**, 605–620, doi:10.1175/JAS-D-15-0167.1.

Kasahara, A., and P. L. Silva Dias, 1986: Response of planetary waves to stationary tropical heating in a global atmosphere with meridional and vertical shear. *J. Atmos. Sci.*, **43**, 1893–1912, doi:10.1175/1520-0469(1986)043<1893:ROPWTS>2.0.CO;2.

Kiladis, G. N., and M. Wheeler, 1995: Horizontal and vertical structure of observed tropospheric equatorial Rossby waves. *J. Geophys. Res.*, **100**, 22 981–22 997, doi:10.1029/95JD02415.

——, ——, P. T. Haertel, K. H. Straub, and P. E. Roundy, 2009: Convectively coupled equatorial waves. *Rev. Geophys.*, **47**, RG2003, doi:10.1029/2008RG000266.

Liebmann, B., and C. A. Smith, 1996: Description of a complete (interpolated) outgoing longwave radiation dataset. *Bull. Amer. Meteor. Soc.*, **77**, 1275–1277.

Nishi, N., 1989: Observational study on the 30–60 day variations in the geopotential and temperature fields in the equatorial region. *J. Meteor. Soc. Japan*, **67**, 187–203.

Radon, J., 1917: Über die Bestimmung von Funktionen durch ihre Integralwerte längs gewisser Mannigfaltigkeiten (The radon transform and some of its applications). *Math.-Phys. Kl.*, **69**, 262–267.

Wallace, J. M., and V. E. Kousky, 1968: Observational evidence of Kelvin waves in the tropical stratosphere. *J. Atmos. Sci.*, **25**, 900–907, doi:10.1175/1520-0469(1968)025<0900:OEOKWI>2.0.CO;2.

Wang, B., and X. Xie, 1996: Low-frequency equatorial waves in vertically sheared zonal flow. Part I: Stable waves. *J. Atmos. Sci.*, **53**, 449–467, doi:10.1175/1520-0469(1996)053<0449:LFEWIV>2.0.CO;2.

Wheeler, M., and G. N. Kiladis, 1999: Convectively coupled equatorial waves: Analysis of clouds and temperature in the wavenumber–frequency domain. *J. Atmos. Sci.*, **56**, 374–399, doi:10.1175/1520-0469(1999)056<0374:CCEWAO>2.0.CO;2.

——, ——, and P. J. Webster, 2000: Large-scale dynamical fields associated with convectively coupled equatorial waves. *J. Atmos. Sci.*, **57**, 613–640, doi:10.1175/1520-0469(2000)057<0613:LSDFAW>2.0.CO;2.

Yanai, M., T. Maruyama, T. Nitta, and Y. Hayashi, 1968: Power spectra of large-scale disturbances over the tropical Pacific. *J. Meteor. Soc. Japan*, **46**, 308–323.

Yang, G.-Y., and B. J. Hoskins, 2013: ENSO impact on Kelvin waves and associated tropical convection. *J. Atmos. Sci.*, **70**, 3513–3532, doi:10.1175/JAS-D-13-081.1.

——, and ——, 2016: ENSO-related variation of equatorial MRG and Rossby waves and forcing from higher latitudes. *Quart. J. Roy. Meteor. Soc.*, **142**, 1488–2504, doi:10.1002/qj.2842.

——, ——, and J. M. Slingo, 2003: Convectively coupled equatorial waves: A new methodology for identifying wave structures in observational data. *J. Atmos. Sci.*, **60**, 1637–1654, doi:10.1175/1520-0469(2003)060<1637:CCEWAN>2.0.CO;2.

——, ——, and ——, 2007a: Convectively coupled equatorial waves. Part I: Horizontal structure. *J. Atmos. Sci.*, **64**, 3406–3423, doi:10.1175/JAS4017.1.

——, ——, and ——, 2007b: Convectively coupled equatorial waves. Part II: Zonal propagation. *J. Atmos. Sci.*, **64**, 3424–3437, doi:10.1175/JAS4018.1.

——, ——, and ——, 2007c: Convectively coupled equatorial waves. Part III: Synthesis structures and extratropical forcing. *J. Atmos. Sci.*, **64**, 3438–3451, doi:10.1175/JAS4019.1.

——, ——, and ——, 2011: Equatorial waves in opposite QBO phases. *J. Atmos. Sci.*, **68**, 839–862, doi:10.1175/2010JAS3514.1.

——, ——, and L. Gray, 2012: The Influence of the QBO on the propagation of equatorial waves into the stratosphere. *J. Atmos. Sci.*, **69**, 2959–2982, doi:10.1175/JAS-D-11-0342.1.

Yano, J.-I., and M. Bonazzola, 2009: Scale analysis for the large-scale tropical atmospheric dynamics. *J. Atmos. Sci.*, **66**, 159–172, doi:10.1175/2008JAS2687.1.